SAND2017-8850R

Sandia National Laboratories

Operated for the United States Department of Energy
by National Technology and Engineering Solutions
of Sandia, LLC.*

Albuquerque, New Mexico 87185-0101
Livermore, California 94551-0969

date: August 14, 2017

to: Distribution

from: Daniel D. Steck (1554), Judith A. Brown (1554), and Kevin N. Long (1554)

subject: Effect of Microstructure Constraints on the Homogenized Elastic Constants of Elastomeric Sylgard/GMB Syntactic Foam

Executive Summary

Previous numerical studies of Sylgard filled with glass microballoons (GMB) have relied on various microstructure idealizations to achieve a large range of volume fractions with high mesh quality. This study investigates how different microstructure idealizations and constraints affect the apparent homogenized elastic constants in the virgin state of the material, in which all GMBs are intact and perfectly bonded to the Sylgard matrix, and in the fully damaged state of the material in which all GMBs are destroyed. In the latter state, the material behaves as an elastomeric foam. Four microstructure idealizations are considered relating to how GMBs are packed into a representative volume element (RVE): (1) no boundary penetration nor GMB-GMB overlap, (2) GMB-GMB overlap, (3) boundary penetration, and (4) boundary penetration and GMB-GMB overlap. First order computational homogenization with kinematically uniform displacement boundary conditions (KUBCs) was employed to determine the homogenized (apparent) bulk and shear moduli for the four microstructure idealizations in the intact and fully broken GMB material states. It was found that boundary penetration has a significant effect on the shear modulus for microstructures with intact GMBs, but that neither boundary penetration nor GMB overlap have a significant effect on homogenized properties for microstructures with fully broken GMBs. The primary conclusion of the study is that future investigations into Sylgard/GMB micromechanics should either force GMBs to stay within the RVE fully and/or use periodic BCs (PBCs) to eliminate the boundary penetration issues. The implementation of PBCs requires the improvement of existing tools in Sandia's Sierra/SM code.

*Sandia National Laboratories is a multimission laboratory managed and operated by National Technology and Engineering Solutions of Sandia, LLC., a wholly owned subsidiary of Honeywell International, Inc., for the U.S. Department of Energy's National Nuclear Security Administration under contract DE-NA0003525.

Introduction

Sylgard/GMB syntactic foam is used as an electronics potting material. In electronics potting, a material is used to encapsulate the electrical components and protect them from shock and vibration. The material studied here consists of a silicone matrix with glass microballoons (GMBs) dispersed throughout. The GMBs allow the material to behave as a crushable foam that can dissipate energy during shock and vibration. A study into this material is important because it is extensively used in the Nuclear Weapons stockpile for electronics potting and in component mechanical shock mitigation. Questions have also arisen from customers as to whether they can omit the GMBs from the potting material[1].

Preliminary studies suggest that the incorporation of GMBs significantly affect mechanical and thermal properties; however, some of these studies were based on an idealized microstructure (needed to facilitate meshing) and structural boundary conditions applied to the microstructure[1,2]. Studies are therefore needed to investigate the effects of these assumptions. This study will investigate only the idealized microstructures (not the structural boundary conditions). The primary objective of this study is to determine the effect of four microstructure idealizations on the homogenized elastic constants of Sylgard/GMB syntactic foam. The four idealizations are detailed below:

1. No Boundary Penetration or GMB-GMB Overlap (None)
2. GMB-GMB Overlap
3. Boundary Penetration
4. Boundary Penetration & GMB-GMB Overlap

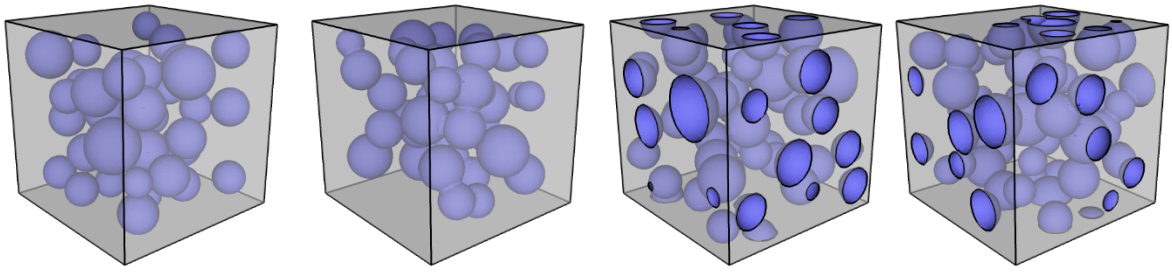

Figure 1. The four microstructure idealizations considered in RVEs in this work

We are interested in boundary penetration and GMB-GMB overlap because other meshing constraints make it impossible to reach volume fractions greater than 20% unless we allow penetration or overlap.

Methodology

The four microstructure idealizations were analyzed at various GMB volume fractions and two material states—in-tact vs. fully broken GMBs. Previous convergence studies showed that RVEs with 40 GMBs showed adequate size convergence such that apparent homogenized elastic constants did not change by more than 5% when compared with larger RVEs (60, 80, 100 GMBs). In this report, all RVEs used 40 GMBs. The simulation matrix is presented in Table 1. Each case was repeated for five microstructure realizations to account

for variability inherent in the microstructure. As seen from the simulation matrix, there is a range of volume fractions that we cannot reach without allowing for boundary penetration. The outputs of each simulation are homogenized bulk modulus and shear modulus.

Table 1. Simulation matrix used for the intact and broken GMB cases

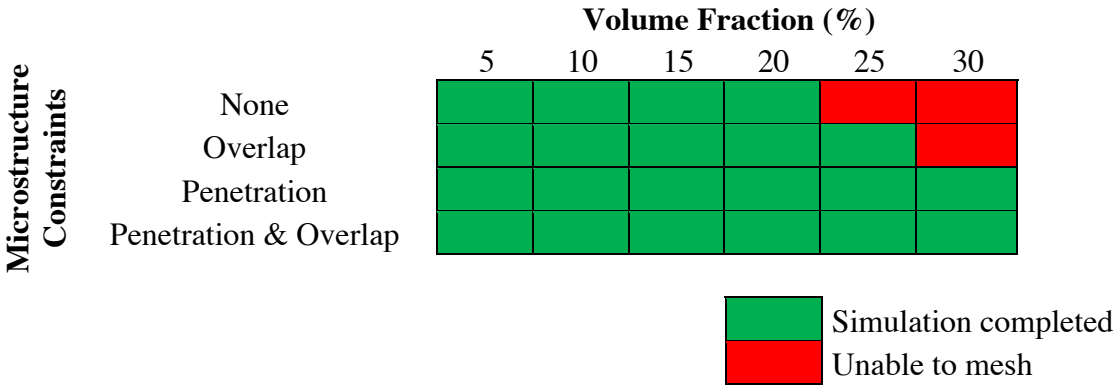

The microstructure model generation process used to obtain each RVE is detailed below:

1. The first step in the process is to generate a list of 40 GMB radii that obey the normal distribution detailed in Figure 2 (μ = 30 microns, σ = 5 microns). A lower bound of 20 microns was imposed to omit the incorporation of statistically improbable GMBs that would greatly diminish the mesh quality. The discrete distribution of radii was then compared against the analytic normal distribution with a Kolmogorov-Smirnov test and required to pass at 95% confidence [3].

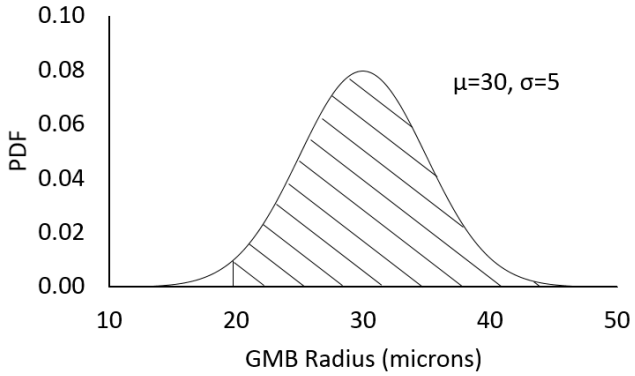

Figure 2. Distribution used to generate a list of GMB radii

2. The second step is to randomly place the GMBs within the volume element. This random placement is subject to constraints required for a high-quality mesh. Specifically, GMBs were required to be separated by a minimum spacing parameter δ between each other and between GMBs and the RVE boundary (for the non-penetrating idealizations). For this analysis δ = 4 microns was used.

3. An automatic meshing tool called Sculpt [4,5] was then used to generate an eight-node uniform gradient hex mesh for the Sylgard matrix. The smallest element size is roughly the size of a 4 micron cube. This element size has been determined to produce mesh-converged results for the homogenized elastic constants through previous studies that considered various element size/ δ ratios. Four node Belytschko-Tsay shell elements were used for the GMBs with 1 micron thickness [6]. The GMB to matrix interface was

modeled as a perfectly bonded contact. Shell elements were used for the GMBs to better represent bending deformation and to reduce the model size. Because the radius to thickness ratio of the GMBs is approximately 30, the shell element idealization is justified. For the fully broken GMB cases, the shell elements were removed from the model.

4. Finally, a linear viscoelastic material model was assigned to the Sylgard matrix [7] and a linear elastic model was assigned to the borosilicate glass GMBs. Borosilicate glass properties of Young's modulus = 61.0 GPa and Shear Modulus = 25.6 GPa were used [8,9].

Figure 3 illustrates the homogenization process used in this study. We are ultimately interested in the effective elastic constants of a macroscale material (left). As the Sylgard/GMB material satisfies necessary scale separation requirements for homogenization [10] (also see Fig. 3), we calculate these from a RVE of the material (middle) where the microscale constituents are explicitly resolved. We perform finite element analysis on the RVE (right) under a suite of boundary value problems (BVP) to calculate the homogenized apparent macroscale elastic constants of the material.

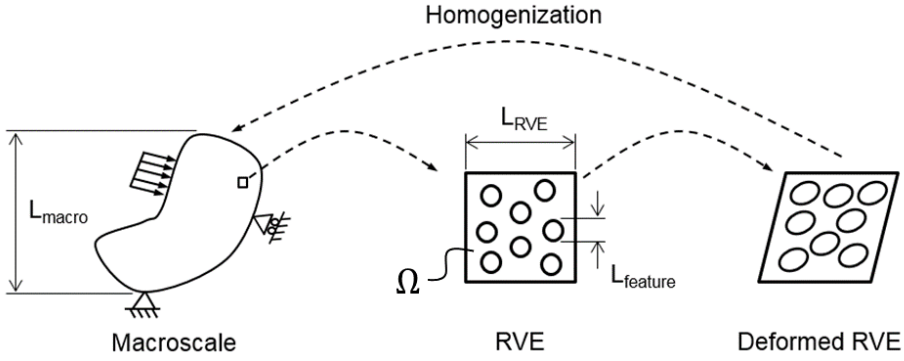

Figure 3. Conceptual overview of computational first order homogenization showing the 3 characteristic length scales required to be substantially different from one another [10]. This scale separation is easily satisfied for the Sylgard/GMB material such that first order homogenization is a viable approach to interrogate the apparent moduli of the macroscale composite.

The boundary conditions imposed on the RVE can take one of several forms: kinematically uniform (KUBCs), statically uniform (SUBCs), or periodic (PBCs). We chose to use KUBCs because current tools available in the Sierra SM finite element analysis suite do not allow us to use periodic boundary conditions and because there is a theoretical issue with homogenizing the void space within the GMBs using SUBCs. Specifically, one cannot volume average the strain within the GMB void space since the strain field is not defined there.

Figure 4 shows how the homogenized elastic constants converge for the three types of BCs. It has been shown that the apparent elastic properties obtained using SUBC give a lower bound on the effective properties, apparent elastic properties obtained using KUBC give an upper bound, and periodic BC produce apparent properties that fall between these two bounds [10,11,12]. The discrepancy between properties obtained from each type of BC is reduced with increasing volume element size, and for a volume sufficiently large to be considered an RVE all types of BC will yield the effective material properties within some tolerance [12]. As stated previously, past studies showed that a RVE with 40 GMBs (studied with 20% volume fraction) shows adequate size convergence within 5% of properties obtained with larger RVEs.

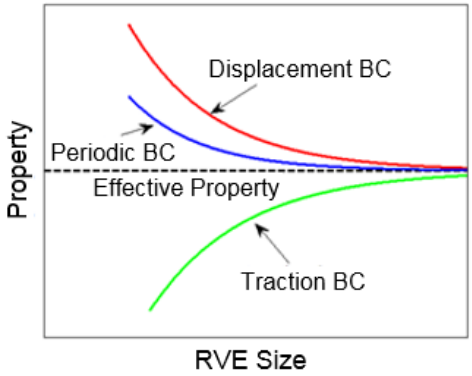

Figure 4. Homogenized apparent property convergence with respect to different types of BCs applied to the RVE[13].

The homogenization procedure is detailed below. All finite element analysis is conducted using the Sierra SM code suite [6].

1. Apply six independent average strains, $\langle \boldsymbol{\varepsilon} \rangle$, to the RVE. This is accomplished by conducting six Boundary Value Problems (BVPs): three independent uniaxial strain BVPs and three independent pure shear BVPs. In each case, we apply a strain with magnitude of 1×10^{-6} to ensure the small strain assumptions inherent in the homogenization theory we use are met. The displacement BC $\{u\}$ required to achive the uniform strain state in each BVP are determined from the expression

$$\{u\} = [E]\{x\},$$

where components of $\{x\}$ are the nodal coordinates. The matrix [E] describes the desired macroscale strain state for the BVP. These displacement conditions are imposed at every node on all the boundaries of the volume element.

2. Volume-average the stress response for each BVP by post-processing the finite element solution obtained in (1) as shown below, where $\boldsymbol{\sigma}(\mathrm{x})$ is the local stress at every point within the RVE, Ω is the domain of the RVE, and $\langle \boldsymbol{\sigma} \rangle$ is the volume averaged stress over the entire RVE domain.

$$\langle \boldsymbol{\sigma} \rangle = \frac{1}{\Omega} \int_{\Omega} \boldsymbol{\sigma}(\mathrm{x}) \mathrm{d}\Omega$$

3. Obtain the apparent stiffness tensor, $\langle \mathbb{C} \rangle$, from the applied average strain, $\langle \boldsymbol{\varepsilon} \rangle$, and the volume-averaged stress response, $\langle \boldsymbol{\sigma} \rangle$, via Hooke's law.

$$\langle \boldsymbol{\sigma} \rangle = \langle \mathbb{C} \rangle \langle \boldsymbol{\varepsilon} \rangle$$

The analysis is designed such that each BVP recovers a separate column of the stiffness tensor. The calculated average stiffness tensor may be slightly anisotropic, but such deviations from known macroscale isotropy in the material are generally much smaller than the recovered values for the isotropic constants [12].

4. Reduce the slightly anisotropic stiffness tensor into an isotropic stiffness tensor by eliminating components that are nearly zero and averaging the other components to obtain a matrix in the standard form seen below, where K is the bulk modulus and μ is the shear modulus. The bulk and shear moduli are then easily calculated from the standard relations for isotropic materials.

$$\langle \mathbb{C} \rangle = \begin{bmatrix} A & B & B & 0 & 0 & 0 \\ B & A & B & 0 & 0 & 0 \\ B & B & A & 0 & 0 & 0 \\ 0 & 0 & 0 & \mu & 0 & 0 \\ 0 & 0 & 0 & 0 & \mu & 0 \\ 0 & 0 & 0 & 0 & 0 & \mu \end{bmatrix}, \text{ where } \begin{cases} A = K + \frac{4}{3}\mu \\ B = K - \frac{2}{3}\mu \end{cases}$$

5. Ensemble average the bulk and shear moduli from the 5 independent microstructure realizations.

Results

Response with In-tact GMBs

The intact GMB bulk modulus results are detailed in Figure 5. The results are grouped by GMB volume fraction and each constraint case is represented by a unique color (as specified in the legend). The error bars in the plot represent the standard of deviation of five microstructure realizations. The key finding that we can extract from Figure 5 is that overlap and penetration independently decrease bulk modulus. This is believed to be caused by the fact that intersecting and partial GMBs are structurally less stiff than perfectly spherical GMBs. The bulk modulus reduction effect is more apparent at higher volume fractions because there is a greater probability of overlap and penetration. GMB-GMB overlap degrades the apparent bulk modulus more than the boundary penetration.

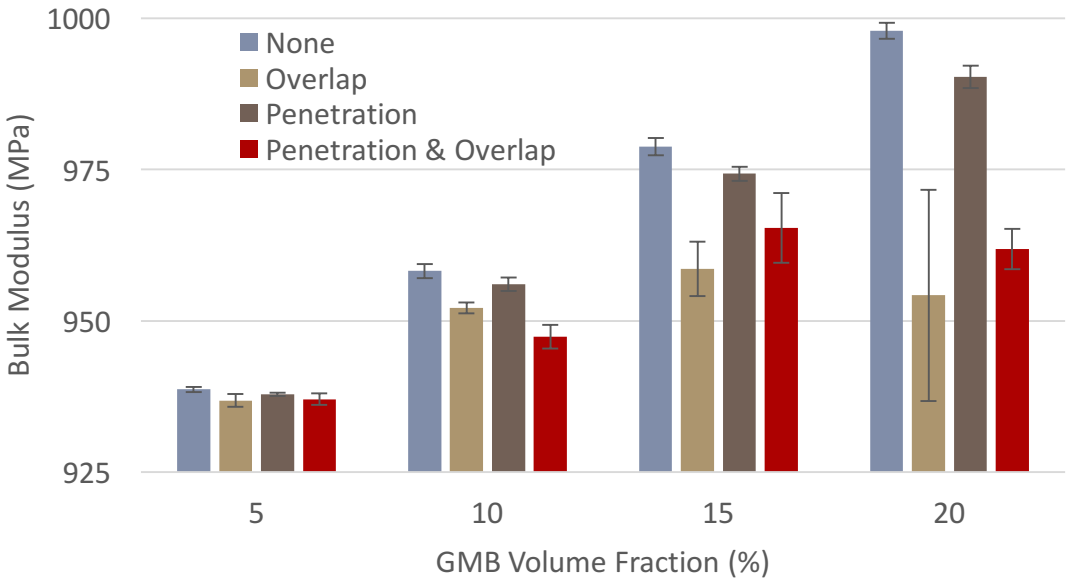

Figure 5. Intact GMB apparent bulk modulus results averaged over 5 independent realizations for all cases

The intact GMB shear modulus results are detailed in Figure 6. The shear modulus plot is laid out in a similar way as the bulk modulus plot. The key finding from Figure 6 is that the boundary penetration greatly increases the apparent shear modulus.

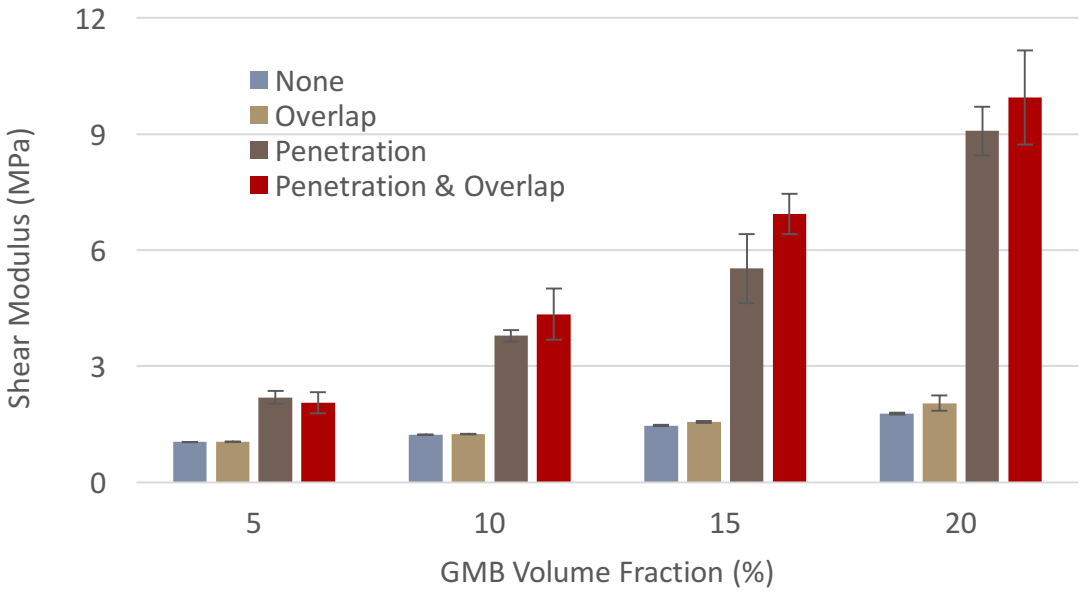

Figure 6. Intact GMB shear modulus results averaged over 5 independent realizations for all cases

This result emerges because the KUBCs excessively deform the GMBs along the boundary. This can be seen clearly in Figure 7 where the GMBs along the boundary are significantly more stressed than those within the matrix. The penetration effect on the shear modulus dominates the bulk modulus effect; the largest variation in bulk modulus presented in Figure 5 is roughly 5% while the largest variation in shear modulus presented in Figure 6 is roughly 500%. This difference is sensible as the bulk behaviors of the matrix phase and in-tact GMB shells is of a similar magnitude while the GMBs are considerably stiffer in shear compared with the Sylgard matrix.

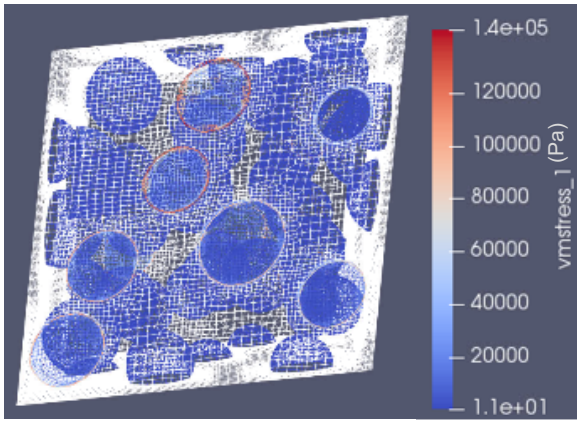

Figure 7. GMB von Mises stress contour plotted on the deformed configuration for the intact GMB case with 20% volume fraction and penetration. The red circles on the boundary show shell elements with artificially high von-Mises stress invariants compared with anything inside the RVE. This result demonstrates an acute boundary effect that stiffens the homogenized stress response and apparent shear modulus.

It should be noted that this effect is specifically related to allowing the stiff inclusion phase (in this material, GMBs) to intersect the RVE boundary while imposing KUBCs. Use of periodic BCs would mitigate this effect by imposing that GMBs intersecting a boundary move in conjunction with their periodic counterpart on the opposite boundary, thus imposing motion that is effectively similar to the GMBs in the RVE interior.

Additionally, we note that the case where both GMB-GMB overlap and boundary penetration are not allowed ("None") produces bulk and shear moduli that are closest to the values and trends predicted previously with analytic composite theory [1,2]. Thus we consider this case to be the most representative of true material behavior. The above results show that when using KUBCs for computational homogenization, the microstructure idealizations of GMB-GMB overlap and boundary penetration produce substantial deviations from this response.

Response with Broken GMBs

The fully broken GMB bulk and shear moduli results are detailed in Figure 8 and Figure 9, respectively. The plots are laid out in the same manner as for the intact GMB cases. The key finding from these plots is that neither boundary penetration nor overlap have a significant effect on the bulk or shear moduli for the fully broken GMB case. This is believed to be due to the fact that there is no hard phase present.

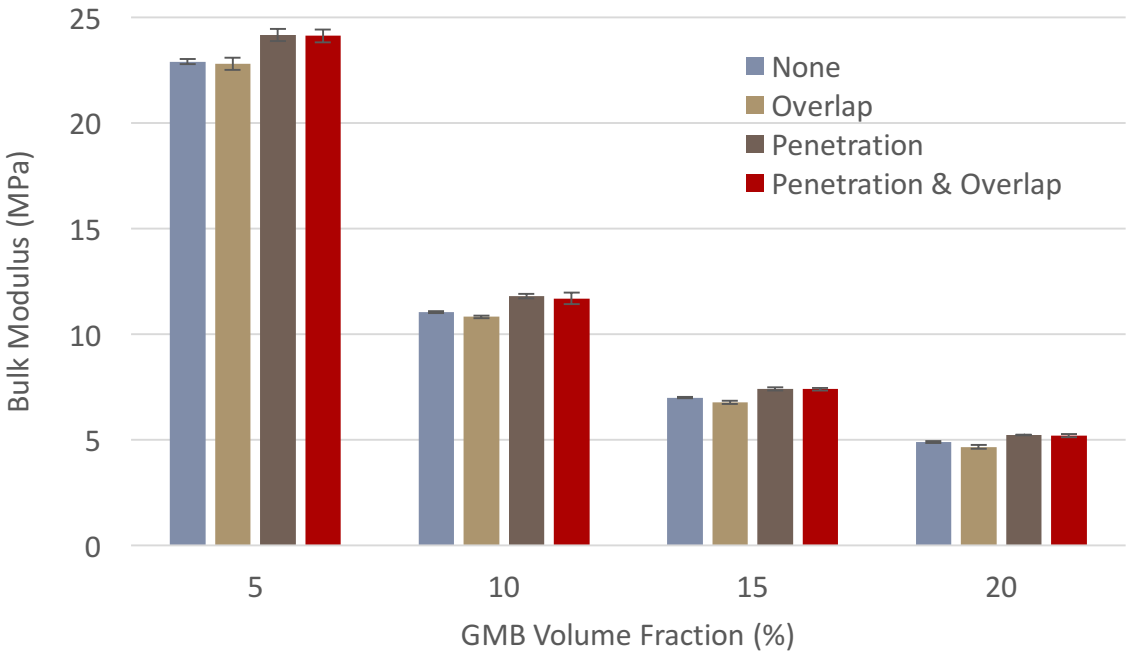

Figure 8. Fully broken GMB bulk modulus results

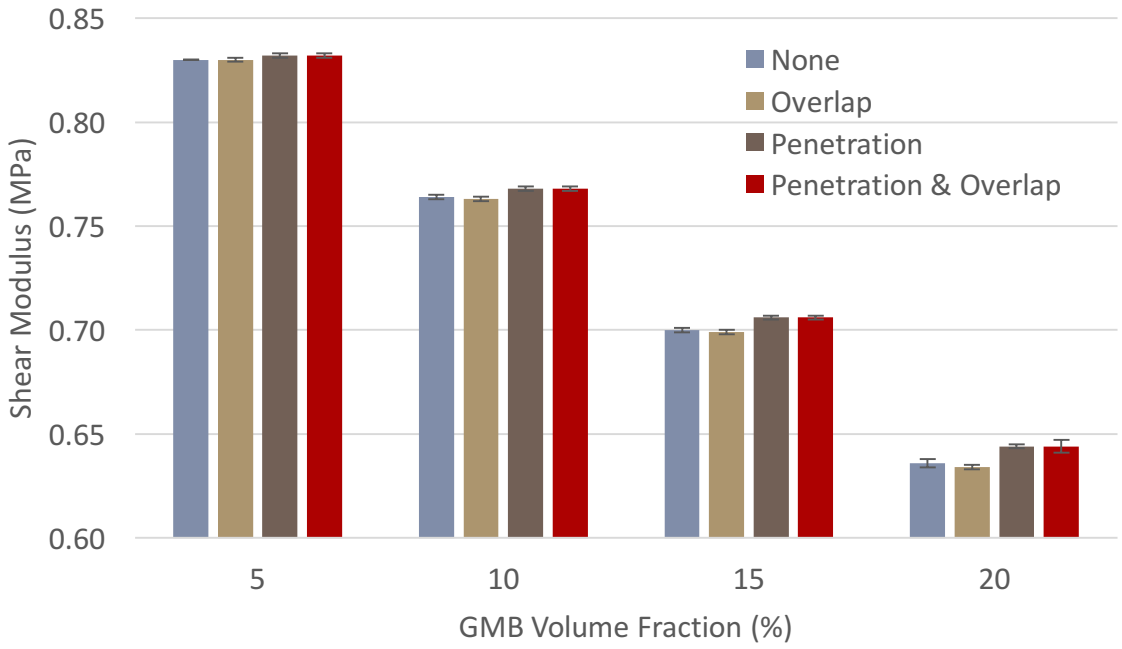

Figure 9. Fully broken GMB shear modulus results

Conclusions

The primary conclusions of the study are listed below:

- Periodic BCs should be implemented for future studies to eliminate the effect of boundary penetration. An alternate approach is to restrict the synthetic microstructures to follow the "None" case (not allowing either GMB-GMB overlaps or boundary penetration), but this is only feasible for GMB volume fractions less than ~20%. Many materials currently in applications of interest have GMB volume fractions much larger than this, so periodic BCs would be necessary to accurately study materials with these higher volume fractions. The implementation of periodic BCs necessitates the improvement of existing tools and may include collaboration with the development team.
- The fully broken GMB cases are relatively insensitive to any of the four microstructure idealizations studied.

References

1. J.A. Brown. Modeling the effect of glass microballoon (GMB) volume fraction on the behavior of Sylgard/GMB composites (SAND2017-4871 R UUR). MEMO (UUR) *SAND2017-4871 R UUR*, Sandia National Laboratories, May 2017.
2. K.N. Long. Elastic constants of sylgard 184 filled with 3m® A16/500 glass microballoons. MEMO *SAND2016-2349 UUR*, Sandia National Laboratories, March 2016.
3. Eric Jones, Travis Oliphant, Pearu Peterson, et al. SciPy: Open source scientific tools for Python, 2001–.
4. Sandia National Laboratories. CUBIT Geometry and Mesh Generation Toolkit User

Documentation, 15.0 edition, August 2017.

5. S.J. Owen, M.L. Staten, and M.C. Sorensen. Parallel hex meshing from volume fractions. In *Proceedings 20th International Meshing Roundtable*, pages 161–178, 2011.
6. Sierra Solid Mechanics Team. Sierra/SolidMechanics 4.44 User's Guide. Computational Solid Mechanics and Structural Dynamics Department Engineering Sciences Center Sandia National Laboratories, Box 5800 Albuquerque, NM 87185-0380, 4.44 edition, October 2016.
7. K.N. Long and J.A. Brown. A linear viscoelastic model calibration for sylgard 184. MEMO *SAND2017-4555 R UUR*, Sandia National Laboratories, April 2017.
8. X. Nie and W.W. Chen. Journal of the American Ceramic Society, 90(8):2556–2562, 2007.
9. S. Chocron, K.A. Dannemann, J.D. Walker, A.E. Nicholls, and Jr. C.E. Anderson. Journal of the American Ceramic Society, 90(8):2549–2555, 2007.
10. S. Nemat-Nasser, M. Hori, *Micromechanics: Overall Properties of Heterogeneous Solids*. North-Holland, Amsterdam, 1993.
11. C. Huet, "Application of variational concepts to size effects in elastic heterogeneous bodies," J. Mech. Phys. Solids 38 (1990), pp. 813-841.
12. T. Kanit, S. Forest, E. Galliet, V. Mounoury, D. Jeulin, "Determination of the size of the representative volume element for random composites: statistical and numerical approach," Int. J. Solids Struct. 40 (2003),pp 3647-3679.
13. T. Kanit, F. Guyen, S. Forest, D. Jeulin, M. Reed, and S. Singleton. Apparent and effective physical properties of heterogeneous materials: Representativity of samples of two materials from food industry. *Computer Methods in Applied Mechanics and Engineering*, 195(33–36):3960 – 3982, 2006.

Internal Distribution

MS-0840 J. Redmond 1550
MS-0840 E. Fang 1554
MS-0840 K. Long 1554
MS-0840 J. Brown 1554
MS-0840 B. Lester 1554
MS-0840 J. Bishop 1554
MS-0840 B. Reedlunn 1554
MS-0840 W. Scherzinger 1554
MS-0840 D. Steck 1554
MS-0845 J. Thomas 1542
MS-0845 M. Merewether 1542
MS-9042 A. Brown 8259
MS-0897 S. Owen 1543
MS-0889 J. Carroll 1851
MS-9957 H. Jin 8343
MS-0346 K. Johnson 1556